On the relationship between relativistic electron flux and solar wind velocity: Paulikas and Blake revisited

Geoffrey D. Reeves,[1] Steven K. Morley,[1] Reiner H. W. Friedel,[1] Michael G. Henderson,[1] Thomas E. Cayton,[1] Gregory Cunningham,[1] J. Bernard Blake,[2] Rod A. Christensen,[1] and Davis Thomsen[1]

Received 30 May 2010; revised 4 October 2010; accepted 19 November 2010; published 17 February 2011.

[1] Thirty years ago Paulikas and Blake (1979) showed a remarkable correlation between geosynchronous relativistic electron fluxes and solar wind speed (Vsw). This seminal result has been a foundation of radiation belt studies, space weather forecasting, and current understanding of solar wind radiation belt coupling. We have repeated their analysis with a considerably longer-running data set (1989–2010) from the Los Alamos National Laboratory energetic particle instruments with several surprising results. Rather than the roughly linear correlation between Vsw and log (flux), our results show a triangle-shaped distribution in which fluxes have a distinct velocity-dependent lower limit but a velocity-independent upper limit. The highest-electron fluxes can occur for any value of Vsw with no indication of a Vsw threshold. We also find a distinct solar cycle dependence with the triangle-shaped distribution evident in 2 declining phase years dominated by high-speed streams but essentially no correlation in 2 solar maximum years. For time periods that do show a triangle-shaped distribution we consider whether it can be explained by scatter due to other parameters. We examine the role of time dependence and time lag in producing the observed distribution. We also look at the same statistical relationship but at energies $\ll$1 MeV. We conclude that the relationship between radiation belt electron fluxes and solar wind velocity is substantially more complex than suggested by previous statistical studies. We find that there are important ways in which the "conventional wisdom" stating that high-velocity wind drives high-MeV electron fluxes is, in general, either misleading or unsupported.

Citation: Reeves, G. D., S. K. Morley, R. H. W. Friedel, M. G. Henderson, T. E. Cayton, G. Cunningham, J. B. Blake, R. A. Christensen, and D. Thomsen (2011), On the relationship between relativistic electron flux and solar wind velocity: Paulikas and Blake revisited, *J. Geophys. Res.*, *116*, A02213, doi:10.1029/2010JA015735.

1. Introduction

[2] In 1979 George Paulikas and Bern Blake published a landmark paper showing the correlation between solar wind velocity (Vsw) and radiation belt electron fluxes [*Paulikas and Blake*, 1979]. They compared the fluxes of >0.7, >1.55, and >3.9 MeV electrons at geosynchronous orbit with solar wind velocity, Interplanetary Magnetic Field (IMF) Ey, sector polarity and other parameters concluding that "when viewed on the time scale of a day or a solar rotation (27 days) or even on the time scale of half a year… the correlation of energetic electron fluxes with solar wind velocities persists." Indeed, the correlation between geosynchronous relativistic electron fluxes and solar wind velocity is one of the best known results in the study of the Earth's radiation belts.

[3] High-speed solar wind can originate from different sources including solar active regions that impulsively eject material in coronal mass ejections (CMEs) and from coronal holes where plasma is free to stream from the solar surface along open magnetic field lines. High-speed streams associated with coronal holes are observed at the Earth most commonly during the approach to solar minimum when coronal holes extend to the solar equator. Equatorial extensions of coronal holes can persist for many solar rotations producing a 27 day recurrence that is commonly used in forecasting radiation belt electron alerts and warnings [see *Williams*, 1966; *Baker et al.*, 1979; *Wrenn*, 1995; *Reeves*, 1998]. Recently much attention has been given to understanding how different solar wind drivers produce different types of responses in radiation belt electron fluxes [see *Borovsky and Denton*, 2006; *Morley et al.*, 2010].

[4] Irrespective of the solar wind source, observations of high-speed solar wind can be used to forecast the flux level

[1]Space Science and Applications Group, Los Alamos National Laboratory, Los Alamos, New Mexico, USA.
[2]The Aerospace Corporation, Los Angeles, California, USA.

This paper is not subject to U.S. copyright.
Published in 2011 by the American Geophysical Union.

for relativistic electrons [*Baker et al.*, 1990]. As one example, Li and colleagues, in a series of papers, demonstrated remarkable accuracy in predicting geosynchronous relativistic electron fluxes using a radial diffusion formulation with free parameters fit to solar wind velocity [see *Li et al.*, 2001, and references therein].

[5] In recent years much theoretical and observational work has been directed at understanding the proximate causes of radiation belt acceleration, transport, and loss. Many of these studies have focused on wave-particle interactions that are "local" in the sense that the waves are generated in the inner magnetosphere and interact with a local "seed population" of electrons. While it is beyond the scope of this paper to provide a review of that body of literature we point readers toward reviews by *Friedel et al.* [2002], *Millan and Thorne* [2007], and *Shprits et al.* [2008]. "Local" acceleration processes that have been studied include linear interaction with VLF whistlers [*Summers et al.*, 1998] nonlinear whistler interactions [*Omura et al.*, 2007], and interaction with other wave modes such as magneosonic waves [*Horne et al.*, 2007]. While there is growing consensus that local acceleration best explains observed phase space density gradients and temporal evolution [*Reeves et al.*, 2009], local acceleration processes are only indirectly tied to solar wind driving through the action of convection and substorms that produce unstable plasma distributions which, in turn, produce the waves that resonantly interact with relativistic electrons. Another body of work focuses on radiation belt acceleration by enhanced diffusion and transport through interaction with ultra low frequency (ULF) waves [*Liu et al.*, 1999; *Mathie and Mann*, 2000; *Rae et al.*, 2005; *Ukhorskiy et al.*, 2005; *Degeling et al.*, 2007]. For these processes, coupling to solar wind velocity is more direct because the source of the ULF waves can be directly tied to velocity fluctuations, pressure fluctuations, Kelvin-Helmholtz instabilities, or other directly driven processes. It is of course possible for both classes of acceleration processes to act simultaneously, sequentially, or preferentially in one event over another. Ultimately, the goal of all these studies, and the primary science driver behind the Radiation Belt Storm Probes (RBSP) mission [*Reeves*, 2007], is predictive understanding of the processes leading to radiation belt acceleration, transport and loss.

[6] In this paper we first describe the data sets used in our study and the methods used to process those data. Next we present the correlations between flux and solar wind velocity (Vsw) by comparing our data to those of Paulikas and Blake and considering the liner and nonlinear correlation coefficients. In section 3.5 we describe the primary features of the Flux-Vsw distribution. In section 3.4 we examine the distribution for a year dominated by high-speed streams and compare with the overall distribution. We next consider whether physical or instrumental flux saturation could contribute to the shape of the distribution (section 3.5) and whether the distribution could be explained by linear correlation with scatter due to other velocity-dependent parameters. In section 3.7 we consider the important contributions of time lag and persistence in the response of radiation belt fluxes to solar wind driving. In section 3.8 we compare years from different phases of the solar cycle and in section 3.8 we present the distribution of fluxes of 62.5 keV fluxes in comparison to the distribution of 1.8–3.5 MeV fluxes before summarizing our conclusions.

2. Data Sets

[7] Now, with long-term data sets of solar wind velocity and geosynchronous electron fluxes, we can revisit the analysis of Paulikas and Blake to further investigate the relationship between solar wind driving and radiation belt electron fluxes. In this study we use nearly continuous relativistic electron data from Los Alamos National Laboratory (LANL) geosynchronous energetic particle instruments and OMNI solar wind data (Figure 1). Our data cover the time from 22 September 1989 to 31 December 2009. Data are available for 7187 days out of this 7405 day (~20.25 year) period.

[8] The observations used here span two solar maxima and two, declining phase, high-speed stream (HSS) phases. The interval also includes the recent period in 2009 when sunspot numbers hovered around zero, 27 day averaged Vsw stayed below ~400 km/s and geosynchronous MeV electron fluxes dropped by nearly an order of magnitude.

[9] Along with sunspot number (SSN), Figure 1 plots 27 day averages of the 1.8–3.5 MeV electron fluxes from the Energetic Sensor for Particles (ESP) [*Meier et al.*, 1996] and 27 day averages of solar wind velocity. Both long-term and event-by-event correlations are readily apparent in Figure 1 and we investigate those correlations in detail in the subsequent sections.

[10] The geosynchronous electron data set that we used here was produced specifically for this study and includes analysis and processing intended to aid long-term studies of geosynchronous electron fluxes. In order to facilitate further analysis and future studies we publish the full data set as auxiliary material to this article and we plan future periodic updates as new data become available.[1] (See *Parsons et al.* [2010] regarding publication of citable electronic data.)

[11] Because of the asymmetry of the geomagnetic field, measured geosynchronous (GEO) electron fluxes exhibit a diurnal variation in intensity based on the local time of the measurement (with higher fluxes typically observed on the day side). Here we publish daily averages which average over 24 h of local time reducing the effects of diurnal asymmetry. Some variation in measurements from different satellites persists due to four factors: (1) satellites at different longitudes pass noon at different times introducing orbit aliasing when the field varies, (2) geosynchronous satellites at different longitudes are at different geomagnetic latitudes and therefore sample different pitch angles and L shells, (3) some instrument-to-instrument variation exists, and (4) individual satellites are not always parked at a fixed geosynchronous longitude for their entire mission life. For all these reasons, we combine daily averages from LANL-GEO Synchronous Orbit Particle Analyzer (SOPA) and Energetic Spectrometer for Particles (ESP) instruments on all seven available satellites.

[12] Satellite 1989–046 has observations that overlap with each of the other six so we use it as a baseline. We use a

[1] Auxiliary material data sets are available at ftp:/ftp.agu.org/apend/ja/2010ja015735. Other auxiliary material files are in the HTML.

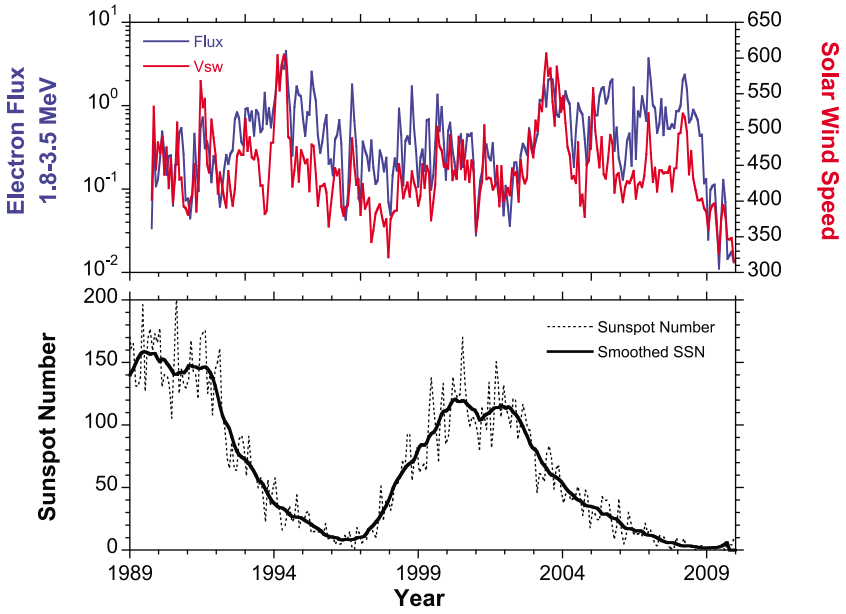

Figure 1. (top) The flux of 1.8–3.5 MeV electrons measured by the LANL-GEO ESP detector (blue) and the solar wind speed, Vsw (red). Both quantities are 27 day averages. (bottom) International sunspot number and smoothed sunspot number.

linear regression to scale simultaneously measured fluxes on each satellite to those measured by satellite 1989–046. We then combine all available satellite data into a single daily average using an average weighted by the error in the linear fit. (See the auxiliary material to this article for the full procedure. We also caution readers that this procedure produces a very uniform time series of electron fluxes, but averages of fluxes over a full day and multiple satellites do not produce realistic energy spectra.)

[13] SOPA data processing includes an additional step. We use a more sophisticated procedure to convert counts to flux. We use Monte Carlo simulations of the instrument response as a function of energy and penetrating backgrounds to fit a relativistic bi-Maxwellian spectrum to the count rates [*Cayton and Tuszewski*, 2005]. The resulting spectrum is evaluated at fixed energies (rather than energy passbands) and fluxes at those fixed energies are daily averaged for each satellite and then merged using the same procedure as for the ESP data.

[14] The analysis here presents data only from the 1.8–3.5 MeV channel on ESP and the 62.5 keV fluxes from SOPA but the auxiliary material contains electron data for channels ranging from 24 keV to 2 MeV. (In the remainder of this document, unless otherwise noted, the term "electron flux" will be used to refer to 1.8–3.5 MeV geosynchronous electron flux.)

[15] Solar wind velocities were computed from the OMNI data set. We use hourly averaged data from the Virtual Radiation Belt Observatory (http://virbo.org) produced using the Qin-Denton algorithm to fill data gaps [*Qin et al.*, 2007].

3. Observations and Analysis

3.1. Solar Cycle Trends

[16] It is already apparent from Figure 1 that there is a clear relationship between solar wind velocity and geosynchronous relativistic electron flux. For solar cycle 22 our observations start near solar maximum with relatively low (27 day average) solar wind velocities as well as low-electron fluxes. As the sunspot number declined the average Vsw and electron fluxes trended upward to a peak in 1994 with 27 day average Vsw exceeding 600 km/s and 27 day average electron flux exceeding 3 × 10° electrons/cm^2/s/sr/keV. After 1994, sunspot number, solar wind velocity, and electron flux all trended lower before increasing again in 1997. Solar wind velocity and electron flux showed quite different phasing in solar cycle 23 than in cycle 22, peaking in late 2002/early 2003 just 1 year after the second peak in sunspot number. Despite the phasing, 2003, like 1994, was characterized by solar coronal holes and periodic corotating high-speed streams (which is apparent in the daily averages but not, of course, in the 27 day averages).

[17] The interval of our analysis ends with a period of highly unusual conditions in the solar wind and geosynchronous electron fluxes. Figure 2 shows daily averages and 27 day averages for the years 2008 and 2009. During this time both solar wind velocities and MeV electron fluxes declined steadily. Average speeds decreased to around 300 km/s and average fluxes decreased by nearly an order of magnitude. We note that even in these apparently anomalous conditions the relationship between geosynchronous electron fluxes and solar wind speeds seem to persist.

3.2. Flux and Vsw Correlations

[18] While clear correlations are apparent in Figures 1 and 2, there are also some exceptions that are worth noting. For one, the absolute magnitudes do not appear to be quite as well correlated as the trends. Note, for example, the intervals in 1995 and 2005 when electron fluxes exceeded 2 (cm^2-s-sr-keV)$^{-1}$ but average solar wind velocities hovered around 450 km/s. In other cases (such as mid 1993) periods of anticorrelation can also be observed. Indeed, in their

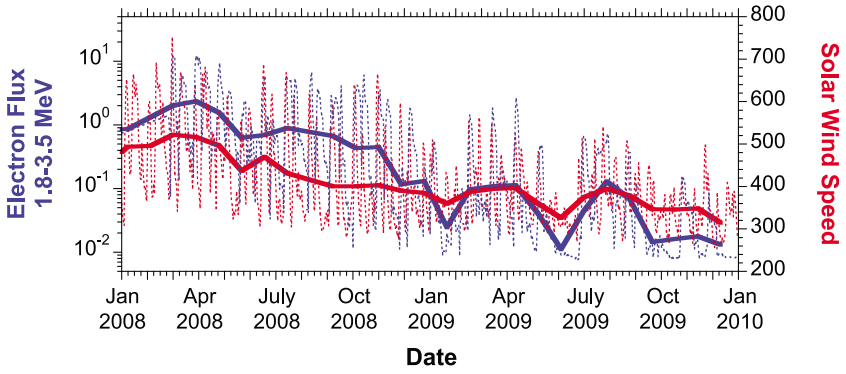

Figure 2. Electron flux and Vsw for the years 2008 and 2009. Daily averages are shown with a dashed line, and 27 day averages are shown with solid curves. During this period both solar wind velocities and geosynchronous electron fluxes declined dramatically yet still show related variations.

original analysis, Paulikas and Blake concluded that factors other than solar wind velocity could likely cause "scatter" in the correlation.

[19] Other authors have further investigated this "scatter." *Blake et al.* [1997] examined in detail a sequence of five events in 1995. They concluded that both density precursors in the solar wind and the orientation of the IMF Bz during the high-speed stream could both exert strong influences on the response of the radiation belts. *Miyoshi and Kataoka* [2008] and *McPherron et al.* [2009], used statistical analyses of stream interaction regions that isolated the effect of IMF Bz dependence. They confirmed that, with other parameters being statistically equal, southward IMF Bz tended to produce a larger response in relativistic electrons to high-speed streams which they attributed to the "Russell-McPherron effect." Other studies have looked at the broad range of solar wind conditions and not specifically at high-speed streams. *Belian et al.* [1996] examined geosynchronous data for a large part of solar cycle 22 showing correlations in long-term trends as well as individual intervals. Similarly *Baker et al.* [2004a] studied an index representing total Radiation Belt Content (RBC) from the Solar Anomalous and Magnetospheric Particle Explorer (SAMPEX) spanning 1992 through 2003 showing that the temporal and statistical relationships between Vsw and radiation belt electron flux are not limited to geosynchronous orbit. *Lyatsky and Khazanov* [2008a] found that the correlation between Vsw and relativistic electron flux improved when the (cube root of) the solar wind density was also considered although correlations still remained low. In a follow-on paper they also considered the effect of geomagnetic activity and concluded that a preceding period of activity strongly increased the correlation but primarily during times of low solar wind density [*Lyatsky and Khazanov*, 2008b]. Many other studies have reached similar conclusions through event studies, superposed epoch studies, and correlations using multiple parameters. Here we present a different analysis that adds new nuance to the interpretation of those previous studies.

[20] Figure 3 reproduces figures from *Paulikas and Blake* [1979] along with similar plots of our observations spanning 1989–2010. The Paulikas and Blake figures show the correlation between >1.55 MeV electron flux and solar wind velocity with averaging times of 36 h, 27 days, and 6 months. Figure 3 (bottom) plots our 1.8–3.5 MeV electron flux data as a function of solar wind velocity using 1 day, 27 day, and 180 day averages.

[21] The correlations in the longer interval of data used in our study suggest a relationship that is more complex than scatter around a linear trend. Linear correlations are typically measured with a Pearson's correlation (often simply referred to as the correlation coefficient). The Pearson's correlation coefficient between solar wind velocity and log (Flux) for our data (1989–2010) are 37% for 1 day averages and 73% for both 27 day and 180 day averages.

[22] A strong feature of the data however, is that the variability of flux at lower Vsw is much larger than the variability in flux at higher Vsw (i.e., the data are heteroscedastic) which violates the assumptions of a Pearson linear correlation. A more appropriate measure of the relationship between log (Flux) and Vsw is given by the Kendall's tau correlation. The Kendall's tau rank orders the variables and measures the number of pairs of variables that increase/decrease together against those that do not [*Sheskin*, 2007]. Therefore the Kendall's correlation can give meaningful correlations to both linear and nonlinear functions. Both the Pearson linear correlation and the Kendall's correlation give a correlation coefficient of 0 for uncorrelated variables and +1 for perfectly correlated variables and −1 for perfectly anticorrelated variables. The Kendall's tau correlation coefficients for our data are 17% for 1 day averages, 46% for 27 day averages, and 52% for 180 day averages.

[23] Our analysis confirms the impression that Figures 1 and 3 give visually, namely that there is a strong relationship between solar wind velocity and relativistic electron flux but that the relationship is not linear and is strongly dependent on the actual value of the solar wind velocity.

3.3. The "Triangle" Distribution

[24] The shape of the distribution of MeV electron fluxes in Figure 3 strongly suggests a triangle. The left hand boundary is easily understood as due to the statistical distribution of daily average solar wind velocities which rarely drop much below 300 km/s. The other two boundaries require further thought.

[25] The "hypotenuse" of the triangle suggests that there is a "soft" lower limit on electron flux that is a strong

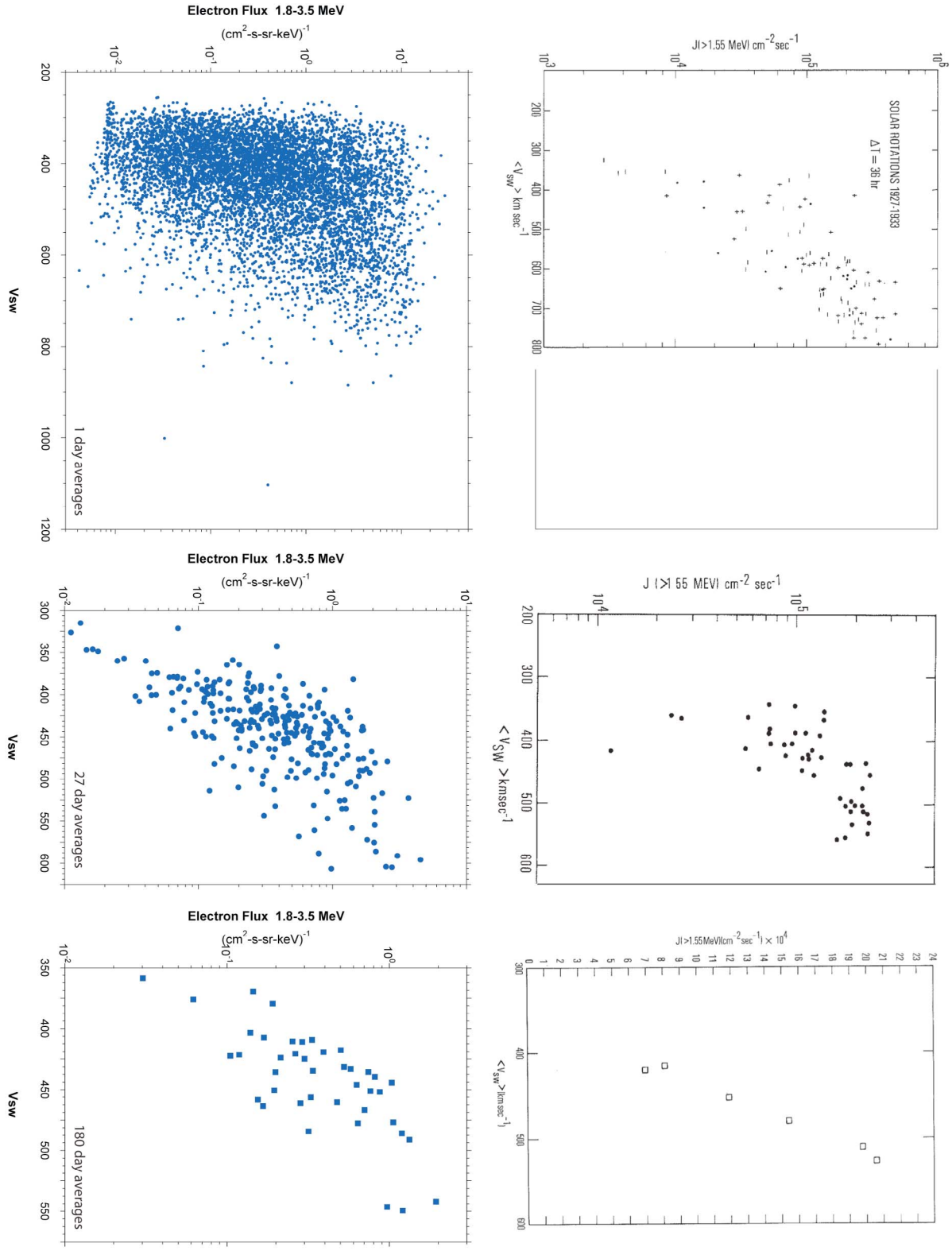

Figure 3. Scatterplots of geosynchronous MeV electron flux and solar wind velocity. (top) Reproduced plots from *Paulikas and Blake* [1979] showing 36 h, 27 day, and 6 month averages for integral energies >1.55 MeV. (bottom) Similar illustrations for our observations spanning 1989–2010. We plot 1 day, 27 day, and 180 day averages of 1.8–3.5 MeV electrons. In our data set, 1 day average solar wind velocities extend to much higher values. The 2 unusually high-velocity days are for the Halloween 2003 storm. The unusually low-velocity points in the 27 day and 180 day are predominately from the years 2008 and 2009 when fluxed often dropped to cosmic ray background levels.

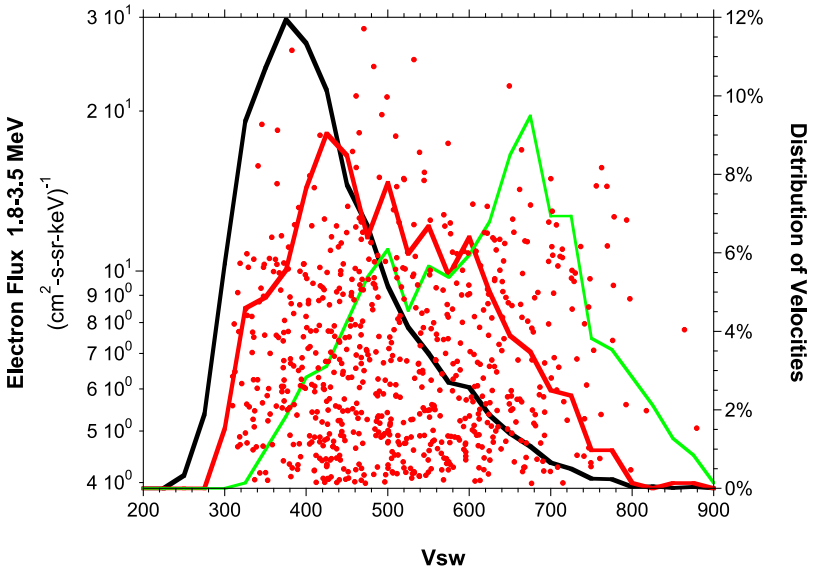

Figure 4. Figure 4 shows the top 10% of all flux values as a function of solar wind velocity (red dots). The most extreme flux levels are observed over a very broad range of velocities. The solid black curve plots the percentage of days as a function of Vsw for all data (i.e., all flux levels). The red curve shows the percentage of days with fluxes in the top 10% as a function of Vsw. The green curve shows the percentage of days with fluxes in the top 10% as a function of Vsw measured 2 days earlier (i.e., with lag). Although extreme flux days tend to have higher velocities than the full data set, the distributions overlap to a remarkable degree.

function of solar wind velocity. For high solar wind velocities we observe consistently high-electron fluxes while low solar wind velocities are associated with a broad distribution of flux levels.

[26] If high solar wind velocities were a requirement, or "necessary condition" for high relativistic electron fluxes then we would expect to see a Vsw-dependent upper limit on fluxes, not a lower limit. If the distribution showed a triangle that was rotated 180° it could be more easily understood. Low fluxes during high-velocity conditions might be understood by invoking lack of other necessary conditions (such as southward IMF Bz) but this is not what is observed.

[27] Instead we find that the highest-electron fluxes are observed under all solar wind conditions. While high solar wind velocities seem to produce high-electron fluxes, low velocities do not imply low fluxes. We emphasize this fact in Figure 4 which shows MeV electron flux as a function of solar wind velocity for the highest-flux days. We show flux as a function of solar wind velocity for the 10% of days that have the highest-flux levels as a scatterplot in Figure 4. (Choosing 10% of the data selects days with flux >3.98 (cm^2-s-sr-keV)$^{-1}$.) Figure 4 also plots the percentage of days with a given solar wind velocity. In black we plot the distribution of Vsw for all 7187 days in our data set. In red we plot the distribution of Vsw for the 719 days that had the highest flux (i.e., 10%). In green we again select the same top 10% flux days but plot the distribution of Vsw observed 2 days prior to the flux measurement. We also tried different subsets of the full distribution including picking the top 2% of all flux values but the results are not sensitive to the precise flux threshold chosen.

[28] There is clearly a tendency for high-flux days to have higher velocities than the overall distribution but it is surprising how weak that tendency is. It is apparent that these high-flux days can occur for any velocity across the entire range. The most probable solar wind velocity for the data set as a whole is 375 km/s. The most probable solar wind velocity for the 10% of days with the highest fluxes is only 425 km/s. The most probable solar wind velocity 2 days prior to the top 10% days is substantially higher at 675 km/s reflecting the well-known fact that electron fluxes tend to peak 2–3 days following the Vsw peak [e.g., *Baker et al.*, 1990]. (We will examine the question of time lag and persistence of fluxes in much more detail in section 3.7.)

[29] In both curves looking at solar wind velocity distributions for the top 10% flux days, a surprising feature is the width of the distribution of velocities. Looking at the red curve in Figure 4 we see that the percentage of high-flux days with Vsw ≈ 350 km/s and the percentage of high-flux days with Vsw ≈ 625 km/s are both about 5%. This means that a day with flux 3.98 (cm^2-s-sr-keV)$^{-1}$ is just as likely to occur on days with mean solar wind velocities of 350 or 625 km/s. Including a lag of 2 days (i.e., the green curve) makes those numbers ≈460 and 740 km/s. In both cases that is a distribution width of nearly 300 km/s.

[30] The other distinct feature in the triangle distribution is the upper limit of flux. One explanation is that the upper limit is caused by local instabilities [*Kennel and Petschek*, 1966]. Other explanations are also possible though. In the following sections we further investigate how this triangle-shaped distribution can be formed and why we see high-flux values over such a large range of solar wind velocities. We have examined several possibilities below and discuss the pros and cons of each interpretation.

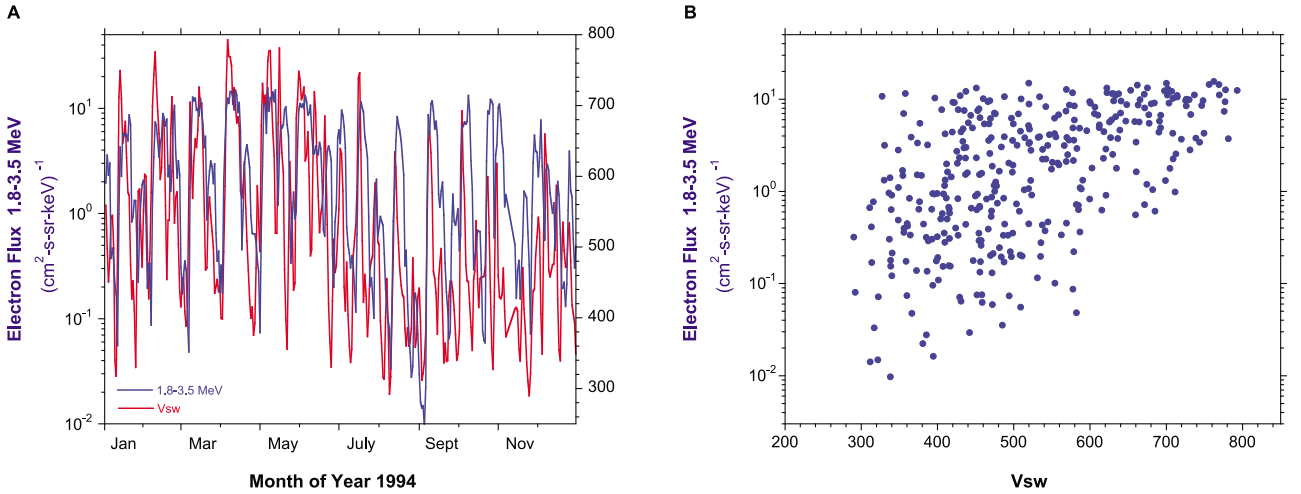

Figure 5. A time series and scatterplot of daily averaged 1.8–3.5 MeV electron flux and Vsw for the year 1994. (a) As the time series shows, 1994 was dominated by recurrent high-speed solar wind streams. The time series suggests a strong relationship between MeV electron flux and Vsw, but (b) the scatterplot shows that the distribution is triangle-shaped rather than linearly correlated.

3.4. High-Speed Streams Versus Other High-Speed Wind

[31] First we examined whether, perhaps, the triangle shape disappeared during the declining phase of the solar cycle when the solar wind was dominated by recurrent high-speed streams. To test this hypothesis we selected the year 1994 when a series of coronal hole associated high-speed streams produced a very coherent radiation belt response [*Reeves*, 1998]. Daily averaged solar wind velocity and 1.8–3.5 MeV geosynchronous electron flux for 1994 are plotted as a time series (Figure 5a) and as a scatterplot (Figure 5b). Clearly Figure 5a shows a strong relationship between electron flux and Vsw. But as Figure 5b shows, the distribution shows the same triangle shape that we saw in the complete 20^+ year distribution. If anything the triangle is even more apparent in this subset of the data.

[32] Figure 6 compares the distribution of flux versus velocity for 1994 with the distribution for all data. (The 2 days during the Halloween 2003 storm with Vsw > 900 km/s are not shown.) Compared with the full data set, the points in 1994 are more heavily weighted toward high solar wind velocity. This is not surprising. We picked 1994 because of the frequent occurrence of high-speed streams. We also see, however, that for intervals of high velocities, say Vsw > 700 km/s, there is more scatter in the full data set than there is for 1994. This suggests that the high-velocity days during high-speed stream intervals produce only high fluxes while high-velocity days under different driving conditions might produce either high fluxes or low fluxes. We will return to this point when we compare different phases of the two solar cycles.

3.5. Flux Saturation

[33] We have noted that the upper limit on flux levels is one of the distinguishing features of the distribution. A flux threshold set by instabilities or other factors would mask what would otherwise be a stronger linear correlation, albeit with more than 3 orders of magnitude variability around the supposed linear trend.

[34] There are two known factors that can limit the upper range of flux values. One factor is local instabilities [e.g., *Kennel and Petschek*, 1966] that can reduce fluxes when they exceed certain limits. The other is count rate saturation in the instrument. It is known that the ESP instrument will saturate at very high count rates (as we discuss in more detail in the auxiliary material). We examined GOES data for 1994 (not shown). The >2 MeV electron distribution is nearly identical to what is seen in the LANL-GEO ESP data

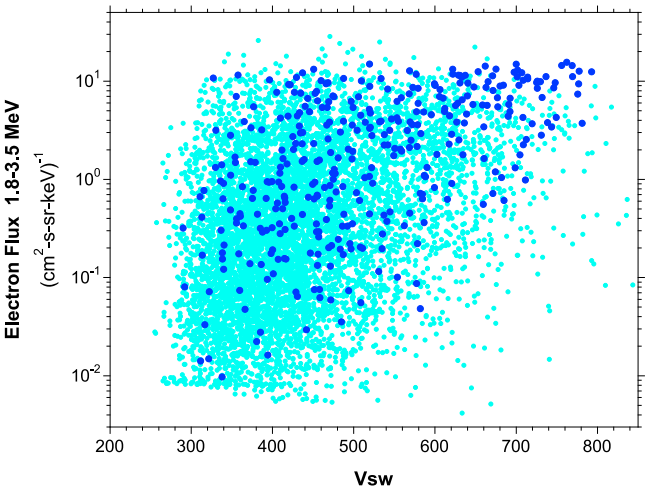

Figure 6. The distribution of daily averaged MeV electron flux and Vsw for 1989–2010 (cyan) and for 1994 (blue). The distribution of points for 1994 has a more distinct triangle shape than the overall distribution. In particular, there is more scatter in the overall distribution at higher velocities than there is for 1994 which suggests that high-speed streams produce a more consistent response than other solar wind structures with equally high average speeds.

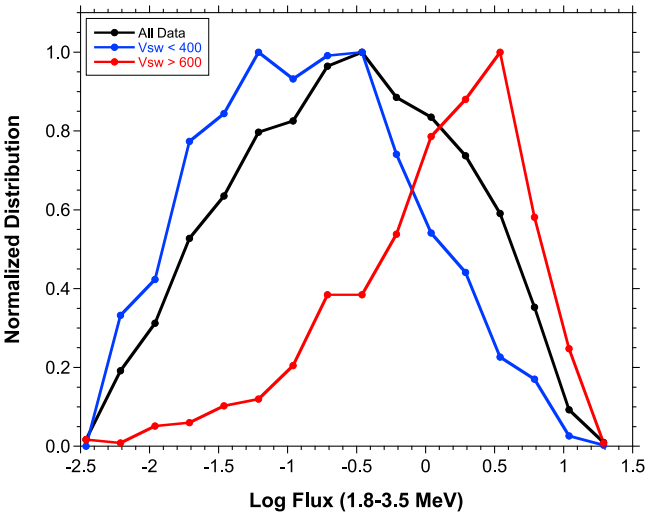

Figure 7. The normalized distribution of MeV electron fluxes. The distribution of days as a function of flux level for all data (1989–2010) is plotted in black. The points are fairly symmetrically distributed around the peak value. The distribution of all days with Vsw < 400 km/s is plotted in blue and shows a slight skewing to lower-flux levels. The distribution of all days with Vsw > 600 km/s is plotted in red and shows a more distinct skewing to higher-flux levels but, again, all three distributions overlap to a very high degree. The distributions also show that any physical instabilities or instrument saturation effects likely have a minimal effect on the overall triangle shape of the distribution of fluxes as a function of Vsw.

but the possible effects of flux saturation in the GOES >2 MeV channel are not known.

[35] We know that both instability and saturation effects do exist but do they explain the shape of the distribution or do they simply "sharpen" the upper edge?

[36] We know that the range of flux variability at low Vsw is about 10^3. If we assume that a similar range of flux variability would exist for all Vsw if flux limits were not acting then for high Vsw, fluxes that "should have" been higher will be instead appear at values near the flux limit. To test this hypothesis we examined the distribution of fluxes in different velocity ranges. If the correlation "should" be linear and the scatter independent of velocity then for high velocities half (or more) of the points should be above the top of the triangle but will "pile up" at some limiting flux.

[37] Figure 7 shows the distribution of log (flux) in different velocity ranges. We show the distribution of fluxes for all solar wind velocities (black), for Vsw < 400 km/s (blue) and for Vsw > 600 km/s (red).

[38] The distributions confirm what the scatterplot suggests. For all solar wind conditions (all years) the distribution is centered near log (flux) = −0.5 (flux in $(cm^2\text{-s-sr-keV})^{-1}$) and is fairly symmetric around that value. For low-velocity solar wind there is a broad distribution but it is somewhat skewed to lower-flux levels. For high-velocity conditions there is a strong tendency for high-flux levels and a distinct lack of low-flux levels. We can see though that the most probable log (flux) value is 0.5 which is at least a factor of 4 lower than the apparent upper flux limit and nearly a factor of 10 lower than the highest-flux values observed. (The distribution of points with the highest fluxes can also be seen in Figure 4.)

[39] We suggest that the case for this hypothesis (i.e., linear correlation + scatter + flux limits) is inconclusive at best. If the hypothesis is true though it does have a very important corollary. It would imply the following: (1) if the saturation is instrumental then actual radiation belt fluxes are much higher than indicated by the instruments or (2) if the saturation is due to instabilities than, in the absence of those instabilities very high speed solar wind would have produced electron fluxes many orders of magnitude higher than what is observed. This, of course, has very profound implications for quantitative theories of how radiation belt electrons are accelerated.

3.6. Velocity-Dependent Controlling Parameters

[40] As we have noted, the distribution of log (Flux) as a function of Vsw is heteroscedastic; the scatter in the distribution is a function of one or more of the variables. We illustrate this schematically in Figure 8.

[41] A distribution with the observed triangle shape could be produced if other parameters that produce the scatter are themselves Vsw dependent. There are certainly candidate parameters (IMF Bz, solar wind density, geomagnetic activity, etc.) but are they likely to produce the observed distribution?

[42] Consider first IMF Bz. The sign and magnitude of Bz have been shown to influence whether or not high-speed solar wind will produce large fluxes. It is unlikely, though, that the influence of Bz can explain the observed distribution. The fraction of time with Bz southward should be about 50% regardless of the velocity of the solar wind. Furthermore, the Bz in high-speed streams is highly variable on time scales shorter than a day [*Tsurutani and Gonzalez*, 1987].

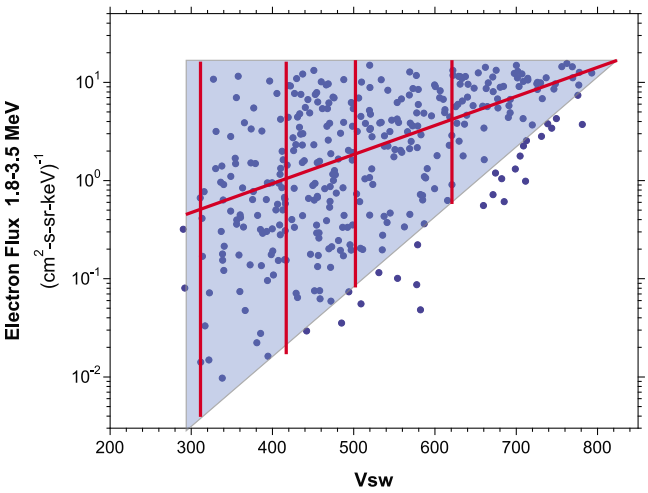

Figure 8. A schematic illustrating a heteroscedastic distribution with a scatter around a linear trend that is dependent on Vsw. Various solar wind properties or geomagnetic processes could produce scatter that is Vsw dependent but most would be more likely to produce distributions with a velocity-dependent upper limit on fluxes rather than a velocity-dependent lower-flux limit.

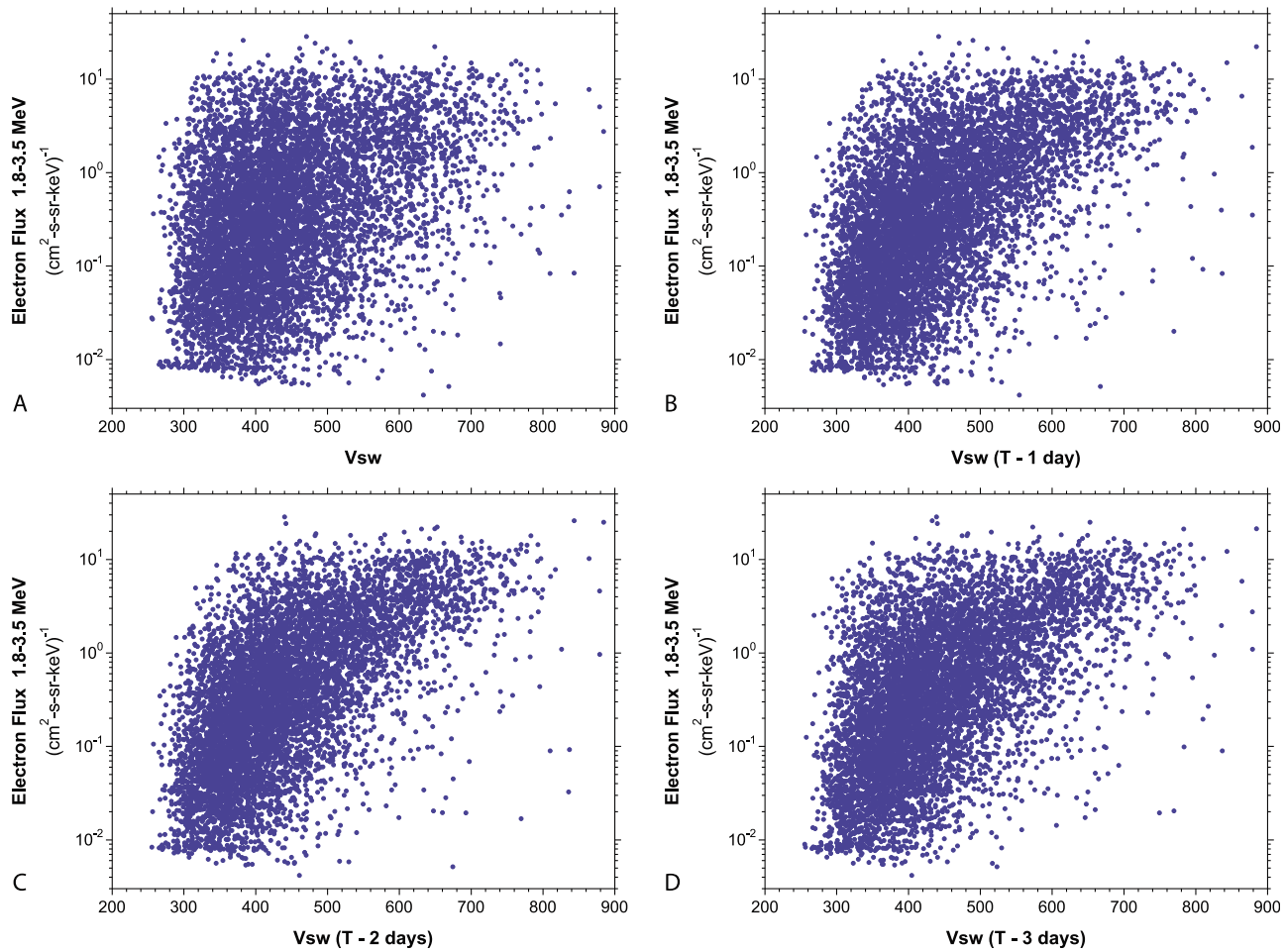

Figure 9. Scatterplots of geosynchronous electron flux as a function of solar wind velocity with various time delays imposed. (a) Simultaneous flux and Vsw. (b) Flux as a function of Vsw on the previous day (T − 1 day), i.e., with 1 day lag with (c) 2 days lag with (d) 3 days lag.

[43] Geomagnetic activity has also been suggested as a controlling parameter [e.g., *Lyatsky and Khazanov*, 2008b]. However, in order for variation in, say Kp, to explain the observed distribution there would have to be more variation in Kp at average solar wind velocities than there is at high solar wind velocities. Similar arguments apply to other variables. It is generally easier to imagine processes that would produce a distribution that has a velocity-dependent upper cutoff than it is to produce a distribution with a velocity-dependent lower cutoff.

[44] We are not, however, suggesting parameters such as IMF Bz, density, Kp, etc. are unimportant variables in understanding radiation belt dynamics. It is just difficult to explain the shape of the observed distribution by only assuming linear correlation between flux and Vsw that is then modulated by those parameters. Studies that investigated the influence of those (and other) parameters certainly have shown that correlations can be improved. However, in those studies even the improved correlations tend to look nonlinear, heteroscedastic, or both.

3.7. Time Dependence

[45] Up to this point we have mainly considered the relationship between simultaneous measurements of the solar wind velocity and the radiation belt electron fluxes. We know, however, that geosynchronous electron fluxes have a coherent response over several days with geosynchronous fluxes typically building up over several days following the arrival of a high-speed stream, CME, or other driver.

[46] It has been noted by many authors, including Paulikas and Blake, that introducing lags in the comparison between electron flux and solar wind velocity can reduce some of the scatter in the plots. *Li et al.* [2005], for example, correlated daily average electron flux (over a range of energies) with various time-lagged solar wind velocities. They examined the linear (Pearson) correlation coefficient as a function of time delay, electron energy, and IMF Bz finding that all three variables affect the value of the correlation coefficient. (That study also used multisatellite LANL data but with somewhat different processing than presented here and the new data sets can be used to reproduce their findings.)

[47] Figure 9 presents a simple analysis with four different lags in the solar wind velocity. (Many other time lag studies can be imagined. We have tested many that we have not included here but those and others can be performed with the supplemental data.) As with previous studies, we found

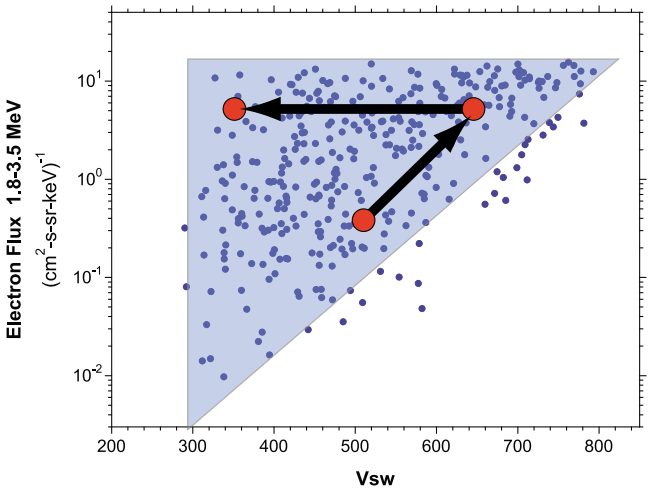

Figure 10. A schematic illustrating a time-dependent pattern of flux changes. If MeV electron fluxes tend to increase under increasing Vsw and then persist at a given flux level as Vsw decreases, it would naturally produce a triangle-shaped distribution. High-flux-low-velocity days could be the result of a lagged response to earlier high-speed solar wind conditions.

that introducing time lags in the correlation can reduce (or enhance) the scatter in the plots. Figure 9 presents scatterplots with time lags of 0, 1, 2, and 3 days. (We also examined time lags of 4 days, 5 days, etc.) We did the analysis on the full data set (1989–2010) as well as subsets of the data such as those presented elsewhere in the paper. As Figure 9 illustrates, the amount of scatter in the plots can be reduced when various time delays are applied. Thus we confirm that the geosynchronous relativistic electron flux is best correlated with the solar wind velocity measured 2 days earlier. The correlation (Kendall's tau values) for lags of 0, 1, 2, 3, and 4 days are 17%, 31%, 35%, 31%, and 24%, respectively.

[48] What is surprising, and not apparent unless the scatterplots themselves are considered, is that the overall features of the triangle distribution remain even in the time delayed correlations. (1) The correlations are definitely not linear and the nonlinear correlation coefficients are statistically significant but not large. (2) There is a clear Vsw-dependent lower limit to electron flux. (3) The upper limit of electron flux is not velocity dependent and extends over a large range of solar wind velocities. Therefore we can conclude (as others have) that time lags are important and likely point toward acceleration and transport processes that require several days to respond to solar wind driving. It is also clear, however, that time delays are a partial explanation but not a complete explanation for the triangle-shaped distribution.

[49] Two additional, well-known features of the response of electron fluxes to Vsw must also be considered. One is that the time lag can vary from event to event. A close examination of Figure 5a shows events for which the electron response is simultaneous to the increase in Vsw as well as events for which the response is delayed. Another factor is persistence of radiation belt response. After an interval of high Vsw, electron fluxes can remain high, or even increase, for several days even as Vsw decreases. One sequence of events that takes into account variable time lags and persistence of electron fluxes is (1) increasing solar wind velocities increase the radiation belt electron fluxes fairly rapidly; (2) once enhanced, electron fluxes remain elevated for several days while the solar wind velocity decreases; and (3) subsequently fluxes may decay or start a new cycle depending on further changes solar wind velocities. This time-dependent cycle is illustrated schematically in Figure 10 and quite naturally produces a triangle.

[50] To test our hypothesis we selected all daily averages with high flux but low solar wind velocities (flux >3.9 (cm^2-s-sr-keV)$^{-1}$ and Vsw < 400 km/s). For 1994 there were 6 days that satisfied these criteria and they are plotted with red points in Figure 11. The 6 high-flux-low-velocity days identify for unique intervals. For each interval we traced backward in time for 5 days as shown by the solid lines. Since we intentionally picked the lowest-velocity days all 4 events show higher solar wind velocity at some point in the previous 5 days but the time histories for these events are not consistent with the sequence of events illustrated in Figure 10 (i.e., lag plus persistence).

[51] We looked at many time histories chosen either at random from different sections of the scatterplot (Figure 5b) or selectively based on solar wind speed and time history (Figure 5a). We found many events that are, in fact, consistent with the lag plus persistence scenario. Some of these events can be spotted by eye in Figure 5b. And, of course, many events that have been analyzed and published in the literature show just such behavior. What we want to draw attention to are that not all events follow the lag plus persistence scenario and that lag plus persistence is a partial,

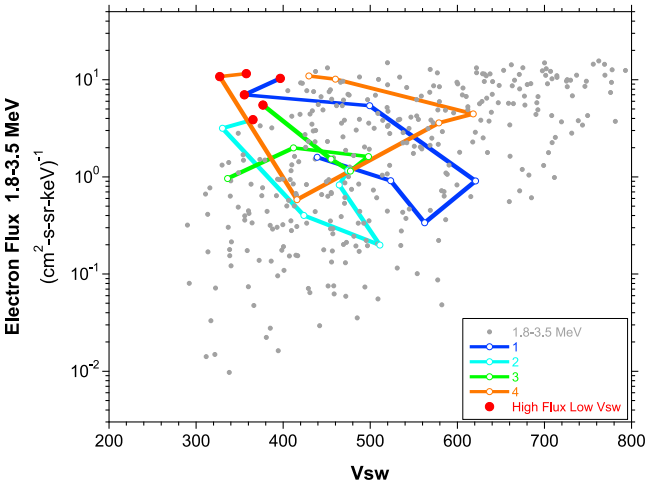

Figure 11. Figure 11 shows flux trajectories as a function of solar wind velocity relative to the overall distribution of points. The red dots show days with high-flux and low solar wind velocity as described in the text. This identifies four distinct intervals. Flux histories for the preceding 5 days are shown with solid curves for each of those intervals (i.e., they trace backward in time from the red dots). While lagged response of fluxes to solar wind velocities and persistence of fluxes are known features of geosynchronous electron fluxes they are not a complete explanation for the shape of the distribution.

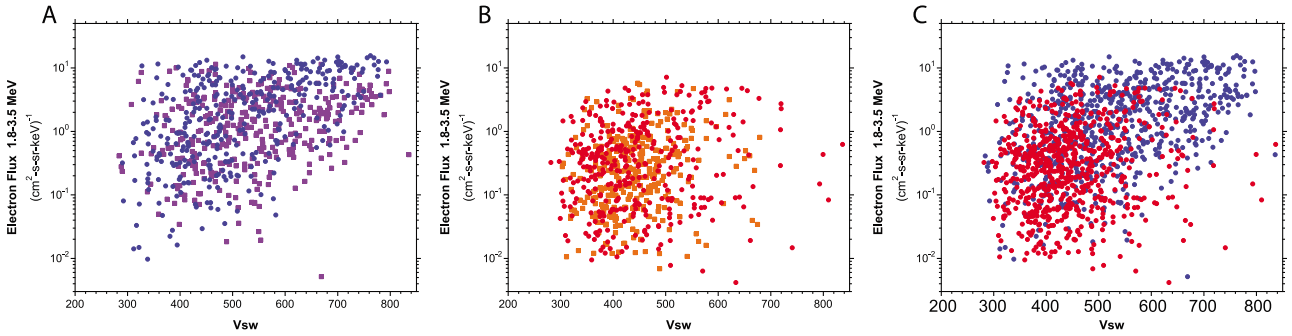

Figure 12. Here we plot 4 years from different phases of the solar cycle. (a) The plot shows the Declining Phase years 1994 (blue) and 2003 (purple) that were dominated by recurrent high-speed streams. Both Declining Phase years show a distinct triangle shape with a large degree of overlap. (b) The plot shows the Solar Maximum years 1990 (orange) and 2000 (red). The distributions for the two Solar Maximum years also quite similar to each other but quite different from the Declining Phase years, showing no statistically significant relationship between MeV electron flux and Vsw. (c) The plot directly compares the two Solar Maximum years (red) with the two Declining Phase years (blue). For every range of solar wind velocities, the distribution of fluxes is different.

but not a complete, explanation for the triangle shape of the log (Flux) versus Vsw distribution.

[52] We also want to draw attention to the points that persistence of fluxes that are decoupled from the initial increase and time lags that vary from event to event are both factors that introduce nonlinearity. Both the nonlinearity and the event-to-event variability need to be better understood than they currently are.

[53] The effects of persistence and variable time lag can both be eliminated if one considers averages over periods of more than a few days. The complicated details of each event should largely disappear in averages over one Carrington rotation of the sun (~27 days) and a number of authors such as *Paulikas and Blake* [1979], *Belian et al.* [1996], and *Baker et al.* [2004a] have considered this. As their studies (and our Figures 1, 2, and 3) show, the correlations are stronger and show less scatter than do daily averages. It is interesting, however, to ponder why the 27 day averages show a distribution that is, in many ways, intermediate between the 180 day and 1 day plots and why the different features of the distributions are or are not present for different averaging intervals.

3.8. Solar Cycle Dependence

[54] We have already determined that the triangle distribution is more prominent during a year dominated by coronal hole-driven high-speed streams (1994) than for the distribution over all conditions (1989–2010). Here we further investigate the distribution seen at different phases of the solar cycle.

[55] Fortunately, the data set that use here includes two declining phases with periods dominated by recurring high-speed streams as well as two solar maxima dominated by impulsively driven solar wind conditions (i.e., CMEs). While we have not yet done a detailed analysis separated by specific solar wind drivers, we present here a comparison of two distinct parts of the solar cycle. The results are shown in Figure 12.

[56] In Figure 12 we again show scatterplots of daily average 1.8–3.5 MeV electron flux as a function of solar wind velocity. We will refer to the years 1994 and 2003 as "Declining Phase" years (Figure 12a) and the years 1990 and 2000 as "Solar Maximum" years (Figure 12b). Figure 1 shows the sunspot numbers, solar wind velocities, and electron fluxes for these 4 years relative to rest of the interval. In Figure 12c we plot all 4 years together for more direct comparison.

[57] The Declining Phase years were chosen specifically because they were dominated by regularly occurring high-speed streams. The two Declining Phase years are plotted with different symbols but the distribution of points is quite similar for both years. It is interesting that 1994 and 2003 overlap very closely. (The 2003 data include the Halloween storm with daily averaged Vsw > 900 km/s driven by a very strong CME [*Baker et al.*, 2004b]. The points for those days are easy to see in Figure 3 but are off scale in these plots.)

[58] The Solar Maximum years, in contrast, show quite a different distribution. Here we see neither a linear correlation nor a triangle distribution. Rather the distribution of points is dominated by the statistical distribution of solar wind velocities. The electron fluxes observed over any given range of solar wind velocities is essentially random and the Kendall's tau is statistically equivalent to zero.

[59] Figure 12c further illustrates the differences between the Declining Phase years and the Solar Maximum years. We see that the high-flux-high-velocity part of the distribution is dominated by the Declining Phase years even though there are some high-velocity intervals in the Solar Maximum years. (Even higher-peak velocities are observed in transient events than is suggested by the daily averages.) What is more striking and more significant is that for any given value of Vsw the distributions of fluxes are clearly different for Declining Phase years than for Solar Maximum years.

[60] It is likely, as noted by many other authors, that it is the long duration, coherent nature of the solar wind conditions associated with high-speed streams that tends to produce higher radiation belt electron fluxes even for the same average solar wind velocities as observed at other times.

[61] It should come as no surprise that the different types of solar wind drivers observed during different phases of the

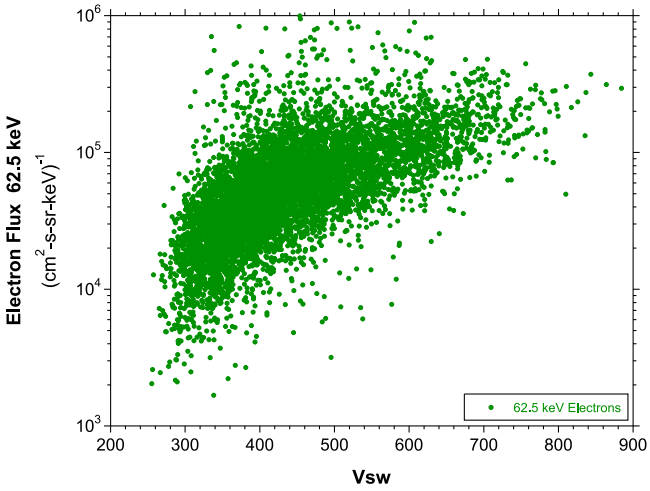

Figure 13. The distribution of 62.5 keV electron fluxes from LANL-GEO SOPA as a function of Vsw for 1989–2010. (Some points are outside the plot limits.) Electrons of these energies are representative of the seed population for the relativistic electrons. Although the distribution of "seed" electrons is not as distinctly triangular as for MeV electrons, it shows very similar features such as a Vsw-dependent lower-flux limit and weak dependence on Vsw for the high-flux points. This leads to the question of whether solar wind velocities control the available seed population for the radiation belts, the intensity of acceleration processes, or both.

solar cycle can produce different radiation belt responses. However, we want to underline two important implications of these results. First, the triangle distribution that is observed for the Declining Phase years of 1994 and 2003 must still be explained in terms of its causal relationship to high-speed stream/CIR structures. The second implication is that during other solar wind conditions (and in particular for solar wind conditions that dominate 1990 and 2000) there is essentially no statistical relationship between relativistic electron fluxes and solar wind velocity at all.

3.9. Source Population Statistics

[62] The majority of studies on this topic have investigated the relationship between Vsw and MeV electrons, i.e., the radiation belts. Paulikas and Blake originally examined electrons with three different integral energy channels: >0.7, >1.55, and >3.9 MeV. Many studies have used GOES data which also provides integral energies and most studies have concentrated on >2 MeV.

[63] Few studies have examined the relationship between Vsw and geosynchronous electron flux as a function of energy. A notable exception is *Li et al.* [2005], who studied cross correlation between geosynchronous electron fluxes at different energies as well as the correlation between electron fluxes and solar wind velocity (lagged and unlagged). They documented the strong correlation of fluxes at different energies ranging from 50 keV to 2 MeV and showed that the time lags were consistent with acceleration from lower to higher energies taking place over several days. The cross correlations with solar wind velocity also showed that low energies have the strongest linear correlation when no lag is applied while higher energies have stronger linear correlation when longer lags are applied. Additionally they showed that the lags and the correlations vary when different IMF Bz criteria are applied.

[64] We have reprocessed the LANL SOPA using Monte Carlo simulations of the instrument response as a function of energy and penetrating backgrounds to fit a relativistic bi-Maxwellian spectrum to the count rates and we have included those data in the auxiliary material. The reprocessed SOPA data allows us to examine the relationship between Vsw and electron flux at energies ranging from 24 keV to 2 MeV from 1989 to 2010. We found that distribution of keV electron fluxes looks remarkably similar to the distribution of MeV fluxes. We illustrate this in Figure 13 which shows flux of 62 keV electrons as a function of Vsw. We were surprised to see again the three characteristic features of the triangle-shaped distribution: (1) correlations that are distinctly nonlinear, (2) a clear Vsw-dependent lower limit to electron flux, (3) and upper limit of electron flux that is not strongly velocity dependent. The upper flux limit is much less sharp for the lower-energy electrons and there are relatively few high-flux-low-velocity days compared to the MeV fluxes. Nevertheless it is clear that whatever solar wind-magnetospheric coupling processes produce these distinctive features must be able to explain the low-energy distribution as well as the high-energy distribution.

[65] Of course, a statistical relationship does not say much about causality. We could interpret Figure 13 as indicating that solar wind velocity primarily affects the seed population of electrons and that the acceleration process may not be Vsw dependent. Alternately, we could interpret the same observations as implying that the tens of keV electrons provide the free energy that control the intensity of acceleration by wave-particle interactions (e.g., whistler chorus). It could be a combination of both.

4. Conclusions

[66] We have examined over 20 years (1989–2010) of solar wind and geosynchronous electron data in order to understand, in more detail, the relationship between solar wind driving and radiation belt response. In particular we examined the correlation between solar wind velocity and 1.8–3.5 MeV electron flux. In doing so we were able to reinterpret the seminal study of *Paulikas and Blake* [1979]. While we confirm that solar wind velocity is a critical parameter for determining radiation belt electron flux the relationship is far from simple.

[67] We found that the correlation between solar wind velocity and the log of geosynchronous MeV electron flux is actually quite low and far from linear. The correlation is primarily driven by a Vsw-dependent lower cutoff in fluxes. The highest-flux days were observed across the full distribution of solar wind velocities. Higher solar wind velocities do give a higher probability for observing the most intense fluxes but, for example, a Vsw of 350 km/s is just as likely to produce flux >3.98 (cm^2-s-sr-keV)$^{-1}$ as a Vsw of 625 km/s.

[68] We suggest that the distribution of geosynchronous electron flux as a function of solar wind velocity is best described by a triangle with a velocity-dependent lower cutoff. While the triangle distribution is observed in the full

data set, it is primarily a feature of coronal hole driven high-speed stream periods such as those that were common in 1994 and 2003. During other solar wind conditions, and in particular for solar wind conditions that dominate 1990 and 2000, there is essentially no statistical relationship between relativistic electron fluxes and solar wind velocity. This suggests that the spatially and/or temporally coherent structures such as CIRs are more effective than other equally fast solar wind conditions at enhancing relativistic electron fluxes as suggested by previous studies [*O'Brien et al.*, 2001].

[69] For the intervals when the triangle distribution does exist (e.g., 1994 and 2003) we still need to understand how the distribution is produced. We examined several possible explanations for the distribution without finding a fully satisfactory answer. It is possible that the distribution is produced because other solar wind and/or geomagnetic parameters moderate the electron response. If so, then the moderating parameters must either be functions of Vsw themselves or an instability that sets an upper flux threshold must substantially narrow the distribution at higher solar wind velocities. While we certainly do believe that parameters other than Vsw are important for determining radiation belt electron fluxes, we do not believe that the "linear correlation plus scatter" hypothesis is a very satisfactory explanation for the observed distribution.

[70] We also examined time lag and persistence as an explanation for the triangle distribution. We do find stronger relationships between flux and solar wind velocity when Vsw is lagged by 1 or 2 days but this is apparently also only a partial explanation for the shape of the overall distribution. In particular the high-flux-low velocity days in 1994 do not show a clear pattern of preceding high-speed solar wind history. Similarly we must ask: Why do some features of the triangle distribution also show up in 27 day averages? How do we explain the high-flux/low-velocity days in the solar maximum years when the highest fluxes occur for Vsw < 600 km/s?

[71] While we do not have a completely satisfying explanation for the triangle distribution we believe that the existence of such a distribution is an important refinement to some 30 years of "conventional wisdom" regarding the relationship between solar wind velocity and radiation belt electron flux. We also come to some striking (and likely controversial) conclusions based on analysis of this distribution.

[72] 1. High solar wind velocity may be a sufficient condition for high radiation belt electron fluxes but it is not a required condition. Even though high Vsw (simultaneous or some days earlier) may be a viable explanation for some points in the distribution, equally high fluxes occur with equal probability for low-Vsw conditions.

[73] 2. There is no specific threshold velocity at which fast solar wind becomes more effective for enhancing geosynchronous electron fluxes; that is, there is no apparent break point in the distribution.

[74] 3. There is a striking solar cycle dependence to the radiation belt responses to solar wind driving conditions, even when we select for intervals with the same solar wind velocities, and, at times, there is no statistical relationship between solar wind velocity and geosynchronous electron fluxes at all.

[75] 4. The relationship between geosynchronous electron fluxes and solar wind velocity is not unique to relativistic electrons. Very similar distributions are observed over a broad range of energies including the radiation belt seed populations at energies <100 keV.

[76] The possibilities we investigated here illustrate interesting examples of possible explanations. Each hypothesis has some aspects that could influence the final distribution but each has arguments against it that make it either unlikely or incomplete. Each test we conducted (including some not shown here) invoked ideas for many more detailed studies that could be done. We have provided the data set in part so that those studies can be done by anyone who wishes to test any other hypotheses or test our hypotheses more rigorously.

[77] **Acknowledgments.** This research was conducted as part of the Dynamic Radiation Environment Assimilation Model (DREAM) project at Los Alamos National Laboratory. We are grateful to the sponsors of DREAM for financial and technical support. We would also like to thank all the individuals who, over the past several decades, have devoted their time and energy to building the SOPA and ESP instruments, supporting their operation in flight, and processing the data archives.

[78] Philippa Browning thanks Mona Kessel and Xinlin Li for their assistance in evaluating this paper.

References

Baker, D. N., R. D. Belian, P. R. Higbie, and E. W. Hones Jr. (1979), High-energy magnetospheric protons and their dependence on geomagnetic and interplanetary conditions, *J. Geophys. Res.*, *84*(A12), 7138–7154, doi:10.1029/JA084iA12p07138.

Baker, D. N., R. L. McPherron, T. E. Cayton, and R. W. Klebesadel (1990), Linear prediction filter analysis of relativistic electron properties at 6.6 re, *J. Geophys. Res.*, *95*(A9), 15,133–15,140, doi:10.1029/JA095iA09p15133.

Baker, D. N., S. G. Kanekal, and J. B. Blake (2004a), Characterizing the Earth's outer Van Allen zone using a radiation belt content index, *Space Weather*, *2*, S02003, doi:10.1029/2003SW000026.

Baker, D. N., S. G. Kanekal, X. Li, S. P. Monk, J. Goldstein, and J. L. Burch (2004b), An extreme distortion of the Van Allen belt arising from the 'Hallowe'en' solar storm in 2003, *Nature*, *432*, 878–881, doi:10.1038/nature03116.

Belian, R. D., T. E. Cayton, R. A. Christensen, J. C. Ingraham, M. M. Meier, G. D. Reeves, and A. J. Lazarus (1996), Relativistic electrons in the outer-zone: An 11-year cycle; their relation to the solar wind, in *Workshop on the Earth's Trapped Particle Environment*, edited by G. D. Reeves, AIP Press, New York.

Blake, J. B., D. N. Baker, N. Turner, K. W. Ogilvie, and R. P. Lepping (1997), Correlation of changes in the outer-zone relativistic-electron population with upstream solar wind and magnetic field measurements, *Geophys. Res. Lett.*, *24*(8), 927–929, doi:10.1029/97GL00859.

Borovsky, J. E., and M. H. Denton (2006), Differences between CME-driven storms and CIR-driven storms, *J. Geophys. Res.*, *111*, A07S08, doi:10.1029/2005JA011447.

Cayton, T. E., and M. Tuszewski (2005), Improved electron fluxes from the synchronous orbit particle analyzer, *Space Weather*, *3*, S11B05, doi:10.1029/2005SW000150.

Degeling, A. W., R. Rankina, K. Kabina, R. Marchanda, and I. R. Mann (2007), The effect of ULF compressional modes and field line resonances on relativistic electron dynamics, *Planet. Space Sci.*, *55*, 731–742, doi:10.1016/j.pss.2006.04.039.

Friedel, R. H. W., G. D. Reeves, and T. Obara (2002), Relativistic electron dynamics in the inner magnetosphere—a review, *J. Atmos. Sol. Terr. Phys.*, *64*(2), 265–282, doi:10.1016/S1364-6826(01)00088-8.

Horne, R. B., R. M. Thorne, S. A. Glauert, N. P. Meredith, D. Pokhotelov, and O. Santolík (2007), Electron acceleration in the Van Allen radiation belts by fast magnetosonic waves, *Geophys. Res. Lett.*, *34*, L17107, doi:10.1029/2007GL030267.

Kennel, C. F., and H. E. Petschek (1966), Limit on Stably Trapped Particle Fluxes, *J. Geophys. Res.*, *71*(1), 1–28, doi:10.1029/JZ071i001p00001.

Li, X., M. Temerin, D. N. Baker, G. D. Reeves, and D. Larson (2001), Quantitative prediction of radiation belt electrons at geostationary orbit based on solar wind measurements, *Geophys. Res. Lett.*, *28*(9), 1887–1890, doi:10.1029/2000GL012681.

Li, X., D. N. Baker, M. Temerin, G. Reeves, R. Friedel, and C. Shen (2005), Energetic electrons, 50 keV to 6 MeV, at geosynchronous orbit: Their responses to solar wind variations, *Space Weather*, *3*, S04001, doi:10.1029/2004SW000105.

Liu, W. W., G. Rostoker, and D. N. Baker (1999), Internal acceleration of relativistic electrons by large-amplitude ULF pulsations, *J. Geophys. Res.*, *104*(A8), 17,391–17,407, doi:10.1029/1999JA900168.

Lyatsky, W., and G. V. Khazanov (2008a), Effect of solar wind density on relativistic electrons at geosynchronous orbit, *Geophys. Res. Lett.*, *35*, L03109, doi:10.1029/2007GL032524.

Lyatsky, W., and G. V. Khazanov (2008b), Effect of geomagnetic disturbances and solar wind density on relativistic electrons at geostationary orbit, *J. Geophys. Res.*, *113*, A08224, doi:10.1029/2008JA013048.

Mathie, R. A., and I. R. Mann (2000), A correlation between extended intervals of Ulf wave power and storm-time geosynchronous relativistic electron flux enhancements, *Geophys. Res. Lett.*, *27*(20), 3261–3264, doi:10.1029/2000GL003822.

McPherron, R. L., D. N. Baker, and N. U. Crooker (2009), Role of the Russell-McPherron effect in the acceleration of relativistic electrons, *J. Atmos. Sol. Terr. Phys.*, *71*(10–11), 1032–1044.

Meier, M. M., et al. (Eds.) (1996), The energy spectrometer for particles (ESP): Instrument description and orbital performance, in *AIP Conference Proceedings*, vol. 383, pp. 203–210, Amer. Inst. Phys., New York.

Millan, R. M., and R. M. Thorne (2007), Review of radiation belt relativistic electron losses, *J. Atmos. Sol. Terr. Phys.*, *69*(3), 362–377.

Miyoshi, Y., and R. Kataoka (2008), Flux enhancement of the outer radiation belt electrons after the arrival of stream interaction regions, *J. Geophys. Res.*, *113*, A03S09, doi:10.1029/2007JA012506.

Morley, S. K., R. H. W. Friedel, E. L. Spanswick, G. D. Reeves, J. T. Steinberg, J. Koller, T. Cayton, and E. Noveroske (2010), Dropouts of the outer electron radiation belt in response to solar wind stream interfaces: Global positioning system observations, *Proc. R. Soc. A*, *466*, 3275–3277, doi:10.1098/rspa.2010.0371.

O'Brien, T. P., R. L. McPherron, D. Sornette, G. D. Reeves, R. Friedel, and H. J. Singer (2001), Which magnetic storms produce relativistic electrons at geosynchronous orbit?, *J. Geophys. Res.*, *106*(A8), 15,533–15,544, doi:10.1029/2001JA000052.

Omura, Y., N. Furuya, and D. Summers (2007), Relativistic turning acceleration of resonant electrons by coherent whistler mode waves in a dipole magnetic field, *J. Geophys. Res.*, *112*, A06236, doi:10.1029/2006JA012243.

Parsons, M. A., R. Duerr, and J.-B. Minster (2010), Data citation and peer review, *Eos Trans. AGU*, *91*(34), 297, doi:10.1029/2010EO340001.

Paulikas, G. A., and J. B. Blake (1979), Effects of the solar wind on magnetospheric dynamics: Energetic electrons at the synchronous orbit, in *Quantitative Modeling of Magnetospheric Processes*, *Geophys. Monogr. Ser.*, vol. 21, pp. 180–202, AGU, Washington, D. C.

Qin, Z., R. E. Denton, N. A. Tsyganenko, and S. Wolf (2007), Solar wind parameters for magnetospheric magnetic field modeling, *Space Weather*, *5*, S11003, doi:10.1029/2006SW000296.

Rae, I. J., et al. (2005), Evolution and characteristics of global Pc5 ULF waves during a high solar wind speed interval, *J. Geophys. Res.*, *110*, A12211, doi:10.1029/2005JA011007.

Reeves, G. D. (1998), Relativistic electrons and magnetic storms: 1992–1995, *Geophys. Res. Lett.*, *25*(11), 1817–1820, doi:10.1029/98GL01398.

Reeves, G. D. (2007), Radiation belt storm probes: A new mission for space weather forecasting, *Space Weather*, *5*, S11002, doi:10.1029/2007SW000341.

Reeves, G. D., A. Chan, and C. Rodger (2009), New directions for radiation belt research, *Space Weather*, *7*, S07004, doi:10.1029/2008SW000436.

Sheskin, D. J. (2007), *Handbook of Parametric and Nonparametric Statistical Procedures*, 4th ed., Chapman and Hall, Boca Raton, Fla.

Shprits, Y. Y., S. R. Elkington, N. P. Meredith, and D. A. Subbotin (2008), Review of modeling of losses and sources of relativistic electrons in the outer radiation belt I: Radial transport, *J. Atmos. Sol. Terr. Phys.*, *70*(14), 1679–1693, doi:10.1016/j.jastp.2008.06.008.

Summers, D., R. M. Thorne, and F. Xiao (1998), Relativistic theory of wave-particle resonant diffusion with application to electron acceleration in the magnetosphere, *J. Geophys. Res.*, *103*(A9), 20,487–20,500, doi:10.1029/98JA01740.

Tsurutani, B. T., and W. D. Gonzalez (1987), The cause of high-intensity long-duration continuous AE activity (HILDCAAs): Interplanetary Alfvén wave trains, *Planet. Space Sci.*, *35*, 405–412.

Ukhorskiy, A. Y., K. Takahashi, B. J. Anderson, and H. Korth (2005), Impact of toroidal ULF waves on the outer radiation belt electrons, *J. Geophys. Res.*, *110*, A10202, doi:10.1029/2005JA011017.

Williams, D. J. (1966), A 27 day periodicity in outer zone trapped electron intensities, *J. Geophys. Res.*, *71*(7), 1815–1826, doi:10.1029/JZ071i007p01815.

Wrenn, G. L. (1995), Conclusive evidence for internal dielectric charging anomalies on geosynchronous communications spacecraft, *J. Spacecr. Rockets*, *32*(3), 514–520, doi:10.2514/3.26645.

J. B. Blake, The Aerospace Corporation, PO Box 92957, Los Angeles, CA 90009, USA.

T. E. Cayton, R. A. Christensen, G. Cunningham, R. H. W. Friedel, M. G. Henderson, S. K. Morley, G. D. Reeves, and D. Thomsen, Space Science and Applications Group, Los Alamos National Laboratory, Los Alamos, NM 87545, USA. (reeves@lanl.gov)